PHYSICAL REVIEW D
PARTICLES AND FIELDS

THIRD SERIES, VOLUME 31, NUMBER 2 15 JANUARY 1985

# Gravitational collapse of a radiating shell of matter

Rick Pim and Kayll Lake
*Department of Physics, Queen's University at Kingston, Ontario, Canada K7L 3N6*
(Received 10 August 1984)

The nonstationary collapse of a radiating fluid shell of matter has been followed through its event horizon in the Vaidya metric in terms of Israel coordinates. The surface density and pressure of the shell were obtained from the integration of the collapse history and are displayed as functions of the shell radius. The shell behavior is determined by two free parameters: its mass function and luminosity-radius relationship. The effects of varying the forms of these two functions have also been examined.

## I. INTRODUCTION

The Vaidya metric[1] has seen considerable recent use at the semiclassical level as a framework for the study of the space-time surrounding an evaporating black hole.[2] In addition, at the classical level, it has seen application as a model for the exterior of quasistationary spherical radiating objects.[3] None of these considerations involve the future event horizon of the Vaidya metric. In fact, while the complete gravitational collapse of a radiating boundary surface has been followed analytically for the case when no event horizon forms,[4] there does not appear to be any attempt in the literature to follow a collapse through the event horizon in the Vaidya metric.

The problem examined in this paper is the complete gravitational collapse of a radiating shell of matter. A Vaidya exterior is matched onto the shell and, in contrast to previous work,[5] the shell is given a surface energy-momentum tensor characteristic of a perfect fluid. As such, it has both a surface density $\sigma$ and pressure $P$. The collapse of the shell is examined within the framework of Israel's complete set of coordinates for the exterior.[6] In this way, the collapse may be followed down to zero radius. The equations required to complete the description of the shell are the luminosity-radius relationship and the Vaidya mass function. Both must be specified, but are not limited to any particular form, so that the choice may be made from the physics of the model rather than mathematical convenience, again in contrast to previous work.[5]

The general approach to the problem used here is fairly straightforward in principle. With the mass function and the luminosity-radius relationship specified, we integrate the equation of motion of a collapsing shell. From the details of the collapse history, we obtain the surface properties of the shell. In practice, the collapse equations we are interested in are very difficult to solve even for very simple (nonphysical) choices of the undetermined functions. As a result, no analytic solution is, in general, possible. The work reported here is, therefore, primarily numerical in nature.

## II. COORDINATES

The line element

$$ds^2=2c\,dv\,dr-[1-2m(v)/r]dv^2+r^2d\Omega^2\,, \tag{2.1}$$

where $c=\pm1$, and $d\Omega^2\equiv d\theta^2+\sin^2\theta\,d\phi^2$ is the Vaidya metric.[1] For $c=-1$ ("outgoing" coordinates) $v$ is a retarded time, while for $c=+1$ ("ingoing" coordinates) it is an advanced time. This provides the solution to the Einstein equations for an energy-momentum tensor of the form

$$T_{\alpha\beta}=qk_\alpha k_\beta\,, \tag{2.2}$$

where $k_\alpha$ is a radial null vector. The function $q$ may be identified with the local radiation energy density. The Vaidya solution, then, describes a "radiating Schwarzschild metric"; a spherically symmetric geometry, but with radial unpolarized radiation around the central mass.

As in the Schwarzschild case,[7] the coordinates $(r,\theta,\phi,v)$ do not adequately describe the entire space-time. For example, if we set $c=-1$ (outgoing coordinates) and consider the behavior of an incoming null geodesic, we find that as $r$ decreases, $v$ diverges. The limiting case is $r=2m(\infty)$ at $v=\infty$. This is analogous to the Schwarzschild surface $r=2m$ at $v=\infty$ the "future" event

 

horizon in Eddington-Finkelstein coordinates.[7] Clearly, a complete set of coordinates is required to describe adequately gravitational collapse.

For the Schwarzschild case a complete set is, for example, Kruskal coordinates.[7] An analogous set, which we refer to as Israel coordinates,[6] exists for the Vaidya metric, but not one that is frequently used. This is quite possibly because, in many respects, Israel coordinates are considerably more complicated than $(r,\theta,\phi,v)$.

Introduce a null coordinate $u$ and consider $m$ to be a $C^2$ nonvanishing function of $u$. The transformations

$$dv = c\,du/U(u),\quad dU(u) = du/4m(u) \tag{2.3}$$

with

$$r = 2m(u) + U(u)w$$

yield the line element

$$ds^2 = 2\,du\,dw + [4m'(u)/U(u) + w^2/2mr]du^2 + r^2 d\Omega^2 , \tag{2.4}$$

where a prime denotes $d/du$. This metric provides an analytic completion to (2.1) that is regular for $r>0$, except on the axis $u=0$ where the metric is $C^0$ (Ref. 8).

The associated Lagrangian for radial trajectories is given by

$$2L = 2\dot{u}\dot{w} + (4m'/U + w^2/2mr)\dot{u}^2 , \tag{2.5}$$

where $2L = -1,0,+1$ represents timelike, null, or spacelike trajectories, respectively. Tangent and normal four-vectors to radial trajectories are

$$u^\alpha \equiv (\dot{u},\dot{w},0,0) \tag{2.6}$$

and

$$n^\alpha = \pm(\dot{u}, -(4m'/U + w^2/2mr)\dot{u} - \dot{w},0,0) . \tag{2.7}$$

The condition $u=$constant defines a family of radial null geodesics parametrized by $w$ so that

$$k^\alpha = (0,1,0,0),\quad k_\alpha = (1,0,0,0) \tag{2.8}$$

defines a radial null vector. The only nonzero component of the Einstein tensor is

$$G_{uu} = G_u{}^w = 2m'/Ur^2 . \tag{2.9}$$

The coordinates, then, represent a solution to the Einstein equations with the "geometrical optics" energy-momentum tensor (2.2), with $q = (1/4\pi r^2)(m'/U)$.

Some of the basic properties of the coordinates can be seen in the limit corresponding to $m$ constant (the Schwarzschild metric).[6] Figure 1 shows the space-time diagram. It shows the properties we expect from the Schwarzschild metric, and possesses some qualities in common with Kruskal coordinates. For example, as in Kruskal coordinates we have the $r=$const curves appearing as a family of hyperbolas: $r = 2m + uw/4m$, or $uw=$constant. In addition, the axes $uw=0$ (and hence $r=2m$) are null surfaces, analogous to the axes in Kruskal coordinates. The geodesic behavior illustrates the differences with Kruskal coordinates. There are two radial null directions at every point, and in Kruskal coordinates radial null geodesics are straight lines. In Israel coordinates, the two families are defined by

$$u = \text{const} \tag{2.10}$$

and

$$dw/du = -w^2/4mr . \tag{2.11}$$

The second class is anything but straight and must be determined by integration.

Israel coordinates illustrate the expected properties of the Schwarzschild geometry, but they are sufficiently complicated as to make the use of them inconvenient. If, however, we examine the case for $m(u)\neq$constant, then we find qualitatively different effects.

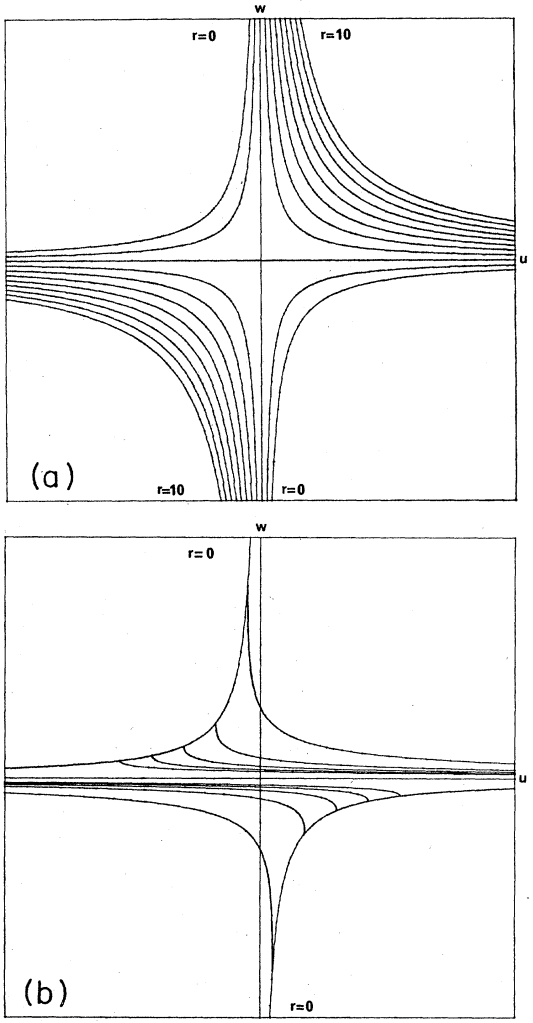


FIG. 1. The Schwarzschild metric in Israel coordinates $[m(u)=1]$. Domain $u=[-4,4]$, range $w=[-50,50]$. (a) This diagram displays the surfaces of constant $r$. Shown are the integral values from $r=0$ to $r=10$, inclusive. Note that $r=2m=2$ lies along the axes $w=0$ and $u=0$, and that $v=-4\ln(u)$ $(c=-1)$. (b) This diagram displays the radial null geodesics obtained from the integration of Eq. (2.11). (The class $u=$constant has not been drawn.) Note that the geodesics do not cross the axis $w=0$. The curve $r=0$ is shown for reference.

For most of this work we will be interested in $m(u)$ decreasing to the future (chosen as $\dot{u}<0$) for $u>0$. To avoid a singularity in the coordinates along $u=0$ we take $m'(0)=0$, [with $m''(0)>0$] defining a local minimum in $m$ at $u=0$ ($v$ infinite). We also take $m(u)=m(-u)$. This is by no means a requirement, but is done here simply for convenience. A mass function chosen according to these criteria is, say,

$$m(u)=(2u^2+1)/(u^2+1)\ . \tag{2.12}$$

This is equal to 2 for large $u$ and decreases smoothly to 1 for $u=0$. This choice also has the property that we have Schwarzschild-type (constant mass) behavior for $u=\infty$, and the deviation from this becomes more pronounced as the system evolves in time (decreasing values of $u$). The corresponding Vaidya geometry is pictured in Fig. 2.

The curves of constant radius illustrate that the coordinate $r$ has a complicated behavior. One of the solutions to $r=2m(0)$ is the null surface $u=0$, representing the future event horizon. Distinct from this is the surface $r=2m(0)$ which is spacelike for $m=m(u)$. In addition, if we consider an $r=$constant curve for $u>0$, we find that it is spacelike for $w<0$, timelike for $w>0$ (the reverse is true for $u<0$), and null as it crosses the $w=0$ axis.

The behavior of null geodesics is also complicated. From Eq. (2.5) we see that there are two radial null directions at every point. The two families of null geodesics are defined by

$$u=\text{constant} \tag{2.13}$$

and

$$dw/du=-(2m'/U+w^2/4mr)\ . \tag{2.14}$$

The behavior of this second class must be obtained by the integration of Eq. (2.14). Some of the curves hit $r=0$ at one end, while the other end asymptotically approaches $w=0$. There is also, however, a set of curves that impacts $r=0$ at both ends. This is a major qualitative difference from the Schwarzschild case. The only reason for this behavior is the presence of the $2m'/U$ term in Eq. (2.14). For $2m'/U$ "sufficiently large," the slope of the curve is sufficient to force it across $w=0$. After this, the curve will inevitably hit $r=0$.

In this latter type of trajectory, there is obviously a maximum value of $r$. The location of this maximum may be determined by examining $r$ along the geodesic as a function of, say, $u$. We obtain

$$r'(u)=2m'+w/4m+Uw' \tag{2.15}$$

which, with Eq. (2.14), implies that the maximum occurs at $w=0$. The axis $w=0$ [corresponding to $r=2m(u)$] then represents an apparent horizon. Obviously, for the type of function $m(u)$ that we have specified, this class of geodesic is limited to a maximum value of $r$ of $2m(\infty)$. Hence, any geodesic that crosses the hypersurface $r=2m(\infty)$ is of the first type, all others hit $r=0$ at both ends. This second type of geodesic does not exist at all in the Schwarzschild metric, it is purely a result of the nonconstant nature of the function $m(u)$.

## III. SHELL STRUCTURE

From the basic geometry we can obtain the equations describing the behavior of the shell. Define $u^i$ to be the (timelike) tangent vector to the shell ($\Sigma$). For a surface energy three-tensor of the form

$$S_{ij}=(\sigma+P)u_iu_j+Pg_{ij}\ , \tag{3.1}$$

and enveloping space-times of the form (2.4), we may derive expressions for the surface properties. It follows that[9]

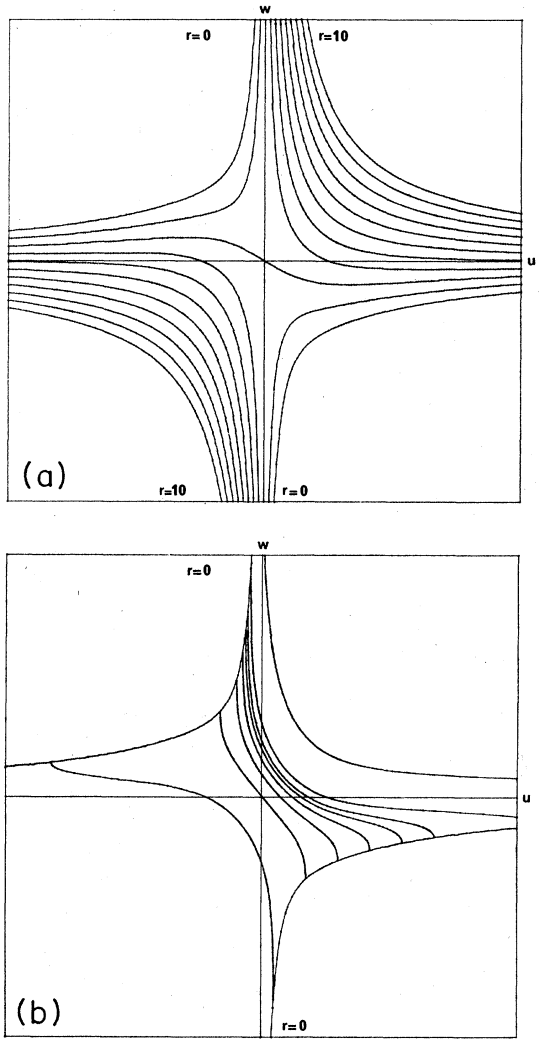


FIG. 2. The Vaidya metric in Israel coordinates with $m(u)$ given in (2.12). Domain $u=[-4,4]$, range $w=[-50,50]$. (a) This diagram displays the surfaces of constant $r$; the figure is analogous to 1(a). Shown are the integral values from $r=0$ to $r=10$, inclusive. As in Fig. 1(a), there are two branches for $r=2m(0)=2$. One is the axis $u=0$, the other is the curve passing through the origin. No simple form exists for the $u\rightarrow v$ coordinate transformation. (b) This diagram displays the radial null geodesics obtained from the integration of (2.14). (The class $u=$constant has again been omitted.) Note that there are two classes of geodesic as described in the text. The space-time is clearly qualitatively different from the Schwarzschild metric [Fig. 1(b)].

$$4\pi R^2\sigma = R[-(\dot{R}^2+1-2m/R)^{1/2}] \tag{3.2}$$

and

$$8\pi P = \left[\frac{R\ddot{R}+\dot{R}^2+1-m/R-\dot{u}^2m'/U}{R(\dot{R}^2+1-2m/R)^{1/2}}\right], \tag{3.3}$$

where $R=r(u)$ is the history of $\Sigma$, the dot represents differentiation with respect to the proper time on $\Sigma$, and, for any $A$, $[A]=(A+)-(A-)$ (evaluated at $\Sigma$).

With the mass function $m$ specified, and Eqs. (3.2) and (3.3), only one more relationship is required. One possible procedure would be to provide an equation of state $[P=P(\sigma)]$ and invert Eqs. (3.2) and (3.3). Alternatively, we might give the history of the luminosity of the shell, and then trace the history of $\sigma$ and $P$. In this paper we use this latter procedure.[10]

From the timelike condition on the Lagrangian for radial trajectories (2.5) we obtain

$$dw/du = -1/2\dot{u}^2 - 2m'/U - w^2/4mr\ , \tag{3.4}$$

where $r$ is given by Eq. (2.3). The jump in the luminosity across $\Sigma$ follows from Eqs. (2.2), (2.6), and (2.7), and is given by

$$4\pi R^2[T_{\alpha\beta}u^\alpha n^\beta] = [m'\dot{u}^2/U] = f(R)\ . \tag{3.5}$$

With $m-=$constant, Eq. (3.5) reduces to the luminosity from $\Sigma$, measured on $\Sigma$. This is the case that is examined here.[11] From Eq. (3.5) we have

$$\dot{u}^2 = Uf(R)/m'\ , \tag{3.6}$$

so that the shell collapse is described by

$$dw/du = -m'/2Uf(R) - 2m'/U - w^2/4mR\ . \tag{3.7}$$

This history is a special case of (3.4), with the details of the shell collapse forced by the choice of the functions $m$ and $f$. For given $f(R)$, $m(u)$, and suitable initial conditions, we integrate (3.7) to follow the collapse of the shell.

Equations (3.2), (3.3), and (3.7) provide all that is required to determine the shell history, but we require values for $\dot{R}$ and $\ddot{R}$. By treating $R$ as a function of $u$ we have

$$\dot{R} = R'(u)\dot{u} = (2m'+w/4m+Uw')\dot{u}\ . \tag{3.8}$$

Since $\dot{u}^2$ is given by (3.6), we have $\dot{R}^2 = R'^2 f(R)U/m'$, which contains no unknown terms.

The remaining requirement is an expression for $\ddot{R}$. Clearly,

$$\ddot{R} = \dot{R}'\dot{u} + R'\ddot{u} = R''\dot{u}^2 + R'\ddot{u}\ . \tag{3.9}$$

The $\ddot{u}$ term is available from Eq. (3.6). Differentiation leads to

$$\ddot{u} = \frac{Uf'(R)R'}{2m'} + \frac{f(R)}{8mm'} - \frac{f(R)Um''}{2(m')^2}\ . \tag{3.10}$$

$R''$ is available from (3.8), as

$$R'' = 2m'' + w'/2m - m'w/4m^2 + Uw''\ . \tag{3.11}$$

An expression for $w''$ is obtained from differentiating (3.7):

$$w'' = \frac{-2(Um''-m'/4m)}{U^2} - \frac{Ufm''-m'(f/4m+Uf'R')}{2U^2f^2} - \frac{2mRww'-w^2(mR'+m'R)}{4m^2R^2} \tag{3.12}$$

which requires no extra information.

In general, there is little chance of finding any analytic solution to (3.7), even for unphysical choices for $m(u)$ and $f(R)$. As a result, Eq. (3.7) is solved here numerically. The method used here is a standard fourth-order Runge-Kutta technique.[12]

## IV. NUMERICAL INTEGRATIONS

We begin with $m+$ given by Eq. (2.12), $m-=0$, and $f(R)=R^2$, corresponding to a luminosity proportional to the surface area of $\Sigma$. Figure 3 gives the results of integrating the collapse trajectories under these conditions from a set of initial points. These histories are timelike, but exhibit similar qualitative properties to the null geodesics of Fig. 2(b). If we trace the trajectories "backwards" ($u$ increasing) we note that there are again two families of curves, one that impacts $R=0$ at both ends, and one that collapses from $R=\infty$. This means that we can have "purely" collapsing shells, as well as some initially expanding. Although the early history of the initially expanding shells is of doubtful physical significance, their evolution is instructive and is included here for clarity.

From the trajectory information the evolution of the shell parameters $\sigma$ and $P$ follows from Eqs. (3.2) and (3.3), and is given in Figs. 4 and 5. Figure 4 describes the $P$ vs $R$ curves along the trajectories of Fig. 3. Note that $P$ is almost always less than zero. In addition, the value of $P$

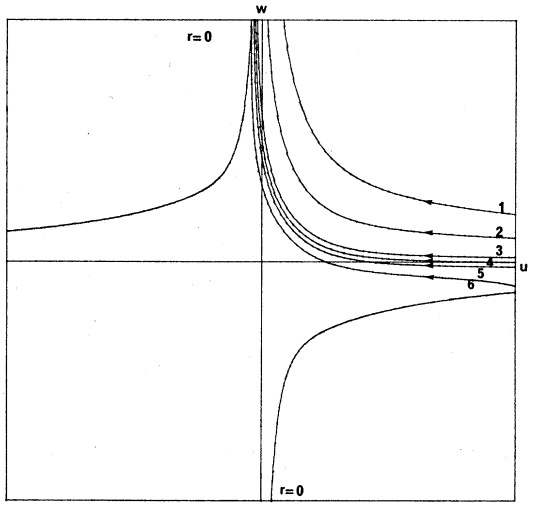


FIG. 3. Shell trajectories in Israel coordinates. A family of trajectories in the $u$-$w$ plane has been plotted for different initial points. The defining form for $m(u)$ is given in Eq. (2.12), while $f(R)=R^2$. Note that the trajectories are labeled for later reference. Two types of behavior are possible. The trajectories labeled 1,2,3 have monotonically decreasing radius, while 4,5,6 are initially expanding.

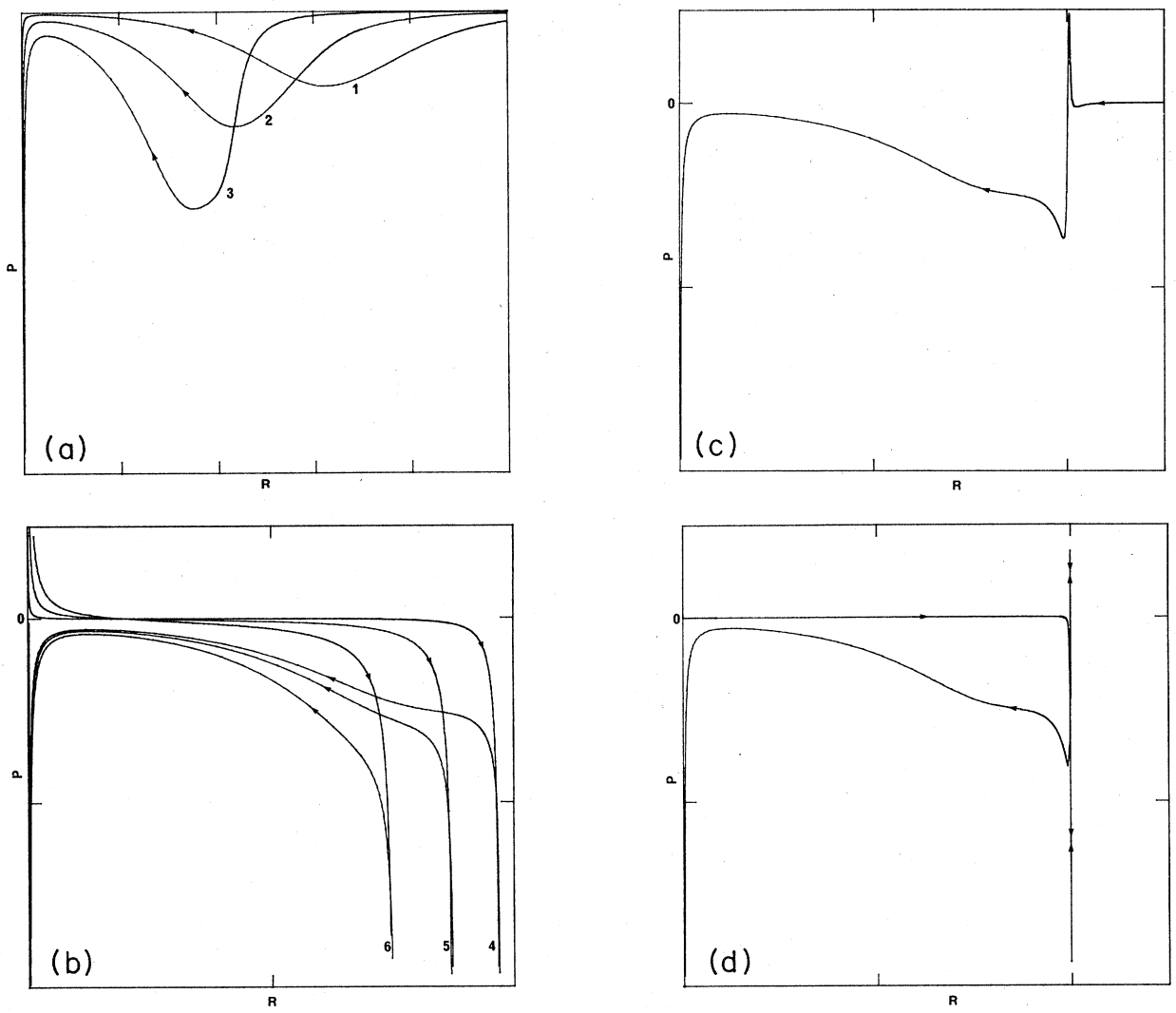


FIG. 4. Variation of $P$ along the shell trajectories. This displays the $P$ vs $R$ variation from Fig. 3. The numbers along the curves correspond to the labels in Fig. 3. (a) $P[-0.1,0]$ vs $R[0,10)]$. This shows the behavior of $P$ along the trajectories marked 1,2,3 in Fig. 3. (b) $P[-0.2,0.05]$ vs $R[0,4]$. This shows the behavior along trajectories 4,5,6. (c) $P[-0.2,0.05]$ vs $R[0,5]$. This shows the behavior along a trajectory "between" 3 and 4. (d) $P[-0.2,0.05]$ vs $R[0,5]$. This shows the behavior along a trajectory "between" 3 and 4.

at any particular value of $R$ is dependent on the history of the collapse, although the limiting cases ($R=0$ and large values of $R$) are the same. Figure 5 gives the corresponding $\sigma$ curves. The density $\sigma$ is, as required, positive, and we also have $\sigma$ depending on the history as well as on $R$. Both figures are traced through the horizon ($u=0$). For our choice of $m(u)$, this corresponds to $R=2m(0)=2$. Note that the units for $\sigma$ and $P$ are not the same on the two figures. The units of $P$ and $\sigma$ are those corresponding to $G=c=1$. mks (or the equivalent) units are not given, as we are not interested in the detailed quantitative nature of $P$ and $\sigma$. In order for the figures to be the same scale, $|P|$ must be reduced by a factor of $c^2$.

$P$ is, as mentioned above, generally negative for all values of $R$, with the large radius limit being zero. From Fig. 4(a) we see that, as $R$ decreases, the magnitude of $P$ increases, and then drops before finally increasing without bound near the singularity ($R=0$). As the initial value of $w$ ($w_0$) along the trajectory (see Fig. 3) decreases, we see a smaller initial value for $|P|$, with a lower local minimum. The second class of trajectories [Fig. 4(b)] initially expands to a maximum value of $R$, then collapses. During the initial expansion, the pressure is positive, then drops below zero for the remainder of the history.

The transition between the curves of Figs. 4(a) and 4(b) may be seen in Figs. 4(c) and 4(d). The $P$ vs $R$ relations are displayed for two "intermediate" trajectories. The behavior of these $P$ curves is quite complicated near $R=4=2m(\infty)$. If we consider a shell collapsing from a large value of $u$ (the "distant past") then $P$ becomes positive and can [in the exact limiting case between the trajectories of Figs. 4(a) and 4(b)] become infinite at

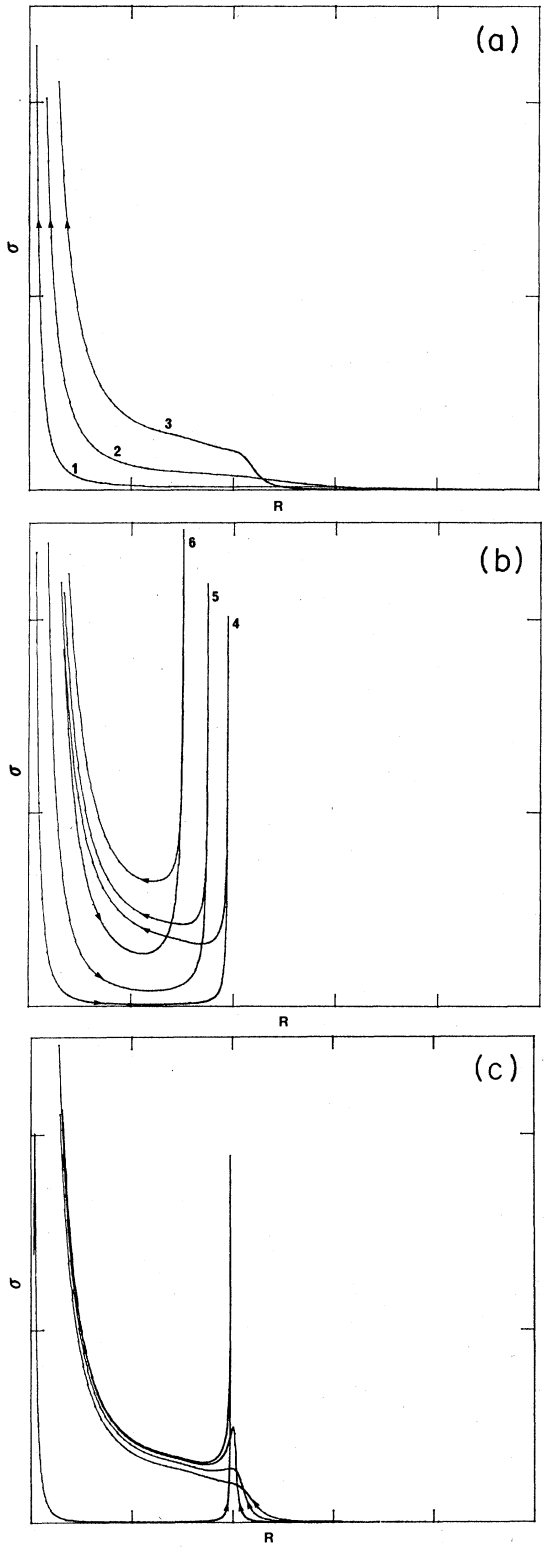


FIG. 5. Variation of $\sigma$ along the shell trajectories. This displays the $\sigma$ vs $R$ variation from Fig. 3. The numbers correspond to the labels of Fig. 3. (a) $\sigma[0,0.025]$ vs $R[0,10]$. This shows behavior along trajectories 1,2,3. (b) $\sigma[0,0.025]$ vs $R[0,10]$. This shows behavior along trajectories 4,5,6. (c) $\sigma[0,0.025]$ vs $R[0,10]$. This shows behavior along the "intermediate" trajectories.

$R=2m(\infty)=4$. In this limiting case, $R=4$ corresponds to $u=\infty$, where $m(u)$ is constant, and $P$ diverges since we are forcing $\Sigma$ to become null.

Figures 5(a) and 5(b) show the companion $\sigma$ curves for the $P$ curves of Fig. 4. For large $R$, $\sigma\to 0$. As $R$ decreases, $\sigma$ increases, eventually diverging at $R=0$. As before, we see an effect near $R=2m(\infty)$. As $w_0$ gets smaller, the "knee" becomes more pronounced until eventually, as before, the second class of curves is obtained.

The exact magnitude and location of the local maximum in $\sigma$ (and the minimum for $P$) in Figs. 5(b) and 4(b) are impossible to locate analytically. It initially appears from the figures that the extremum occurs at the maximum of $R$, but this is in fact not the case. [Note that the "peaks" on the $P$ curves of Fig. 4(b) extend off the bottom of the figure. This is also true for the cases discussed below. On all figures, however, $\sigma$ and $P$ are finite for $R>0$, except in the limiting case discussed above.]

The overall qualitative behavior is not dependent on the exact form of $m(u)$ that we have chosen. If we take, say, $m+(u)=2-\operatorname{sech}(2u)$, then there are no qualitative changes in the properties of the shell. The effect of modifying $f(R)$, is, however, larger. Another possible choice for $f(R)$ might reflect, say, constant luminosity on $\Sigma$: $f(R)=1$. With changes in $f(R)$ there are changes in the shell properties (see Figs. 6 and 7). The nature of the extrema in $P$ and $\sigma$ becomes more obvious—they do not occur at the maximum of $R$. In addition, the magnitude of $P$ is significantly less than for $f(R)=R^2$ and $P$ does not become positive for small values of $R$ [as in Fig. 4(b)]. The detailed behavior of $\sigma$ and $P$ is clearly different.

## V. SUMMARY AND DISCUSSION

The problem examined here has been the complete gravitational collapse of a radiating object which forms an event horizon. The Vaidya metric, which describes the space-time to the exterior of a radiating object, is much more complicated than the Schwarzschild metric. The problem is, in fact, of sufficient difficulty that a relatively simple model for the radiating object, that of a radiating shell with flat interior, has been used in order to accomplish a detailed collapse history. The collapse scenario has been examined using a complete set of coordinates for the Vaidya metric, the Israel coordinates, because "conventional" Vaidya coordinates do not fully cover the entire space-time manifold.

The shell equations derived are complete up to two undetermined functions. One, the exterior mass function, was taken as decreasing to the future from an initial (Schwarzschild-type) constant value. The other, the luminosity function, was taken to be proportional to the square of the shell radius in one case and independent of it in another. Given these two parameters, we have obtained the family of collapse trajectories in Israel coordinates for the Vaidya metric. For these trajectories the surface properties (surface density $\sigma$ and surface pressure $P$) were obtained. There are two classes of trajectories, representing two different types of history for the shell. The first represents a monotonic collapse from a large value of $R$.

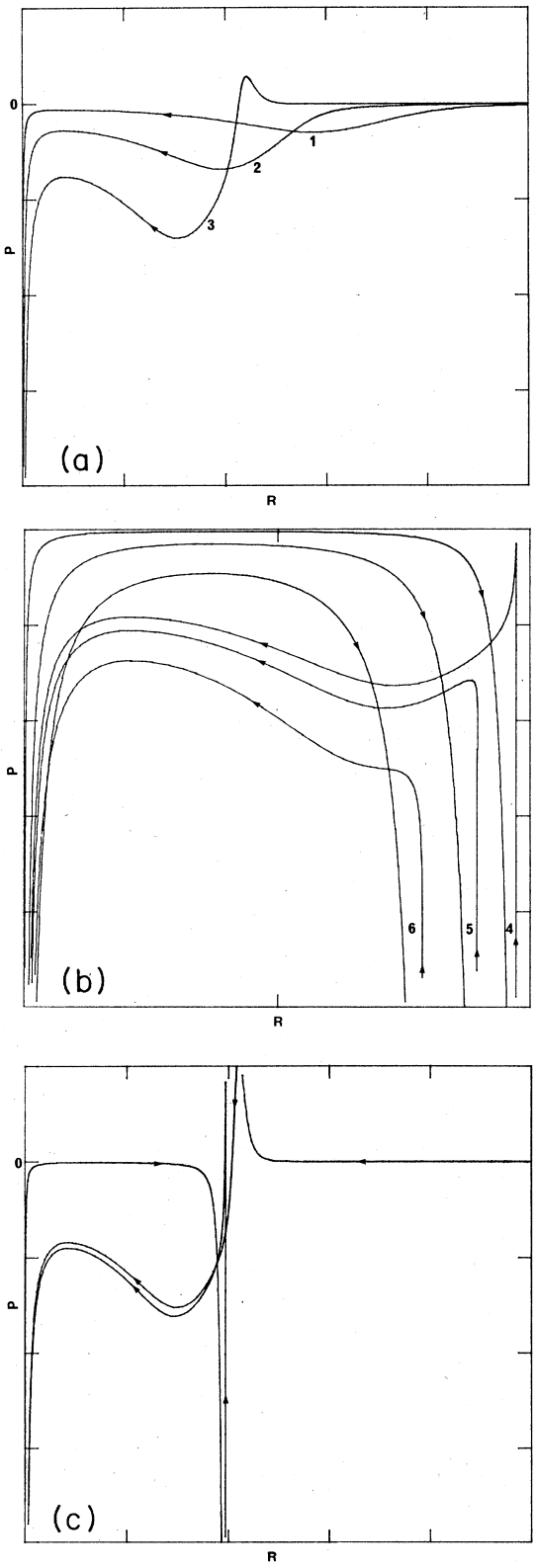


FIG. 6. Variation of $P$ along the shell trajectories. This displays the $P$ vs $R$ relationship for the alternate choice of $f(R)=1$. (a) $P[-0.04,0.01]$ vs $R[0,10]$. Trajectories 1,2,3. (b) $P[-0.05,0]$ vs $R[0,4]$. Trajectories 4,5,6. (c) $P[-0.04,0.01]$ vs $R[0,10]$. Trajectories "between" 3 and 4.

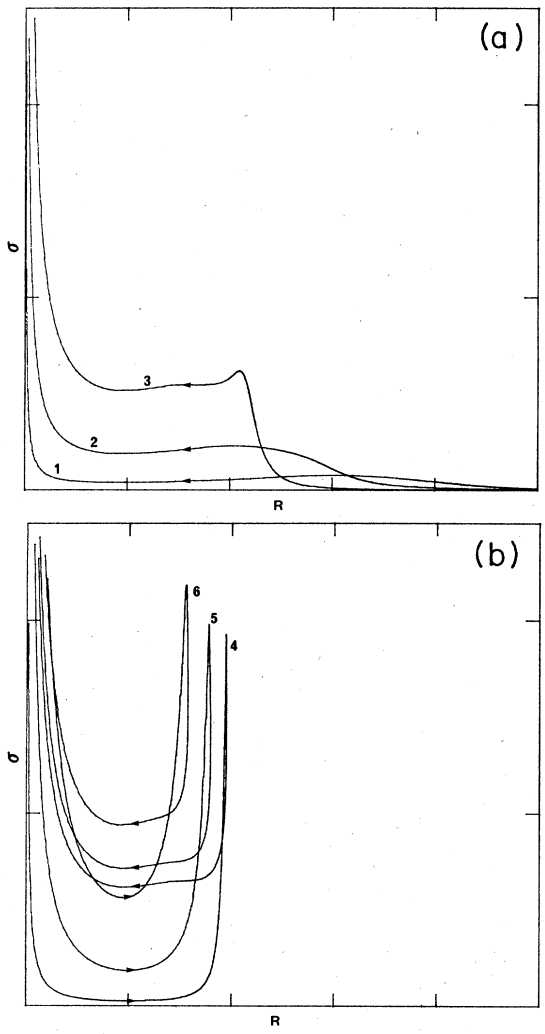


FIG. 7. Variation of $\sigma$ along the shell trajectories. This displays the $\sigma$ vs $R$ relationship for the alternate choice of $f(R)=1$. (a) $\sigma[0,0.025]$ vs $R[0,10]$. Trajectories 1,2,3. (b) $\sigma[0,0.025]$ vs $R[0,10]$. Trajectories 4,5,6.

The second corresponds to a shell that is initially expanding, expands to some maximum radius, and then collapses down to $R=0$.

It has been shown that $P$ is generally, but not always, less than zero.[13] Some general properties of the $\sigma$, $P$ curves are as follows. For monotonic collapse, $\sigma$ increases as $R$ decreases. There is a knee in the curve near $R=2m(\infty)$ which increases in height with decreasing values of $w_0$. There is a local minimum in $P$, again near $R=2m(\infty)$. The depth of this minimum increases with decreasing $w_0$. For trajectories "close to" the second class, the behavior near $R=2m(\infty)$ becomes somewhat exaggerated. The limiting case has $P\to\infty$ at $R=2m(\infty)$ as expected.

The second class is slightly different. We see that the maximum value of $R$ occurs near the axis $w=0$ $[R=2m(u)]$. The surface pressure becomes large and negative, and the shell does not expand significantly

beyond $R=2m(u)$. In addition, for periods of large acceleration ($\ddot{R}$) in the shell's history, the pressure is positive. A positive surface pressure is needed to drive the initial expansion, at least for the $f(R)\propto R^2$. The collapsing section of the curves is quite similar to the curves in the first case.


## ACKNOWLEDGMENTS

One of us (R.P.) would like to thank Queen's University for a Carl Reinhardt Fellowship. This work was supported by the Natural Sciences and Engineering Research Council of Canada.


---


[1]See, for example, R. W. Lindquist, R. A. Schwartz, and C. W. Misner, Phys. Rev. **137**, 1364 (1965).

[2]Note that such considerations frequently use an inflow of negative energy density to cause the evaporation. See, for example, P. Hajicek and W. Israel, Phys. Lett. **80A**, 9 (1980); W. Hiscock, Phys. Rev. D **23**, 2813 (1981); **23**, 2823 (1981); W. Hiscock, L. Williams, and D. Eardley, *ibid.* **26**, 751 (1982).

[3]S. Bayin, Phys. Rev. D **19**, 2838 (1979); **21**, 2433 (1980); L. Herrera, J. Jiminez, and G. Ruggeri, *ibid.* **22**, 2305 (1980); M. Cosenza, L. Herrera, M. Esculpi, and L. Witten, *ibid.* **25**, 2527 (1982).

[4]K. Lake and C. Hellaby, Phys. Rev. D **24**, 3019 (1981); K. Lake, *ibid.* **26**, 518 (1982).

[5]See, for example, V. Hamity and R. Gleiser, Astrophys. Space Sci. **58**, 353 (1978); M. Castagnino and N. Umerez, Gen. Relativ. Gravit. **15**, 625 (1983); V. Hamity and R. Spinosa, *ibid.* **16**, 9 (1984). They do not consider collapse through the event horizon. In addition, the model is completed by various simplifying assumptions. For example, Hamity and Gleiser specify a $P=0$ dust shell with luminosity proportional to shell radius.

[6]W. Israel, Phys. Lett. **24A**, 184 (1967); Phys. Rev. **143**, 1016 (1966).

[7]See, for example, C. W. Misner, K. S. Thorne, and J. A. Wheeler, *Gravitation* (Freeman, San Francisco, 1973).

[8]This deficiency does not, however, affect the present analysis in any way.

[9]Equations (3.2) and (3.3) follow from the more general expressions given by K. Lake, Phys. Rev. D **19**, 2847 (1979), with the use of the coordinate transformation formulas (2.3).

[10]This approach does not work in the limit of the Schwarzschild metric, where one must revert to the specification of an equation of state.

[11]Hamity and Gleiser (Ref. 5) use an expression equivalent to the condition that $f\propto R$. Castagnino and Umerez (Ref. 5) pointed out that this is not what one would expect from the physics of the system, and derive a more general set of equations, leaving the luminosity unspecified. Their subsequent calculations, however, are performed using the original $f\propto R$ relationship.

[12]See, for example, L. Johnson and R. Riess, *Numerical Methods* (Addison-Wesley, Reading, Mass., 1977).

[13]Negative surface pressures are not, in fact, unexpected. We have $[p]=[G_{\alpha\beta}n^{\alpha}n^{\beta}]/8\pi=\sigma\tilde{K}_{\tau\tau}+(2P/R^2)\tilde{K}_{\tau\tau}$ where $p$ is the four-pressure at $\Sigma$. Let $[p]\equiv -2a/R$, so that $a$ is the "surface tension." It follows that $P\rightarrow -a$ in the weak-field, slow-motion limit, $\dot{R}\ll 1$, and $m\pm\ll R$.